

Constraining CMB-consistent primordial voids with cluster evolution

H. Mathis^{1*}, J. Silk¹, L. M. Griffiths² and M. Kunz³

¹*Astrophysics, University of Oxford, Denys Wilkinson Building, Keble Road, Oxford OX1 3RH, UK*

²*Astrophysics, UNSW, Sydney, NSW 2052, Australia*

³*Astronomy Centre, University of Sussex, Brighton BN1 9QJ, UK*

29 November 2018

ABSTRACT

Using cosmological simulations, we make predictions for the distribution of clusters in a plausible non-gaussian model where primordial voids nucleated during inflation act together with scale-invariant adiabatic gaussian fluctuations as seeds for the formation of large-scale structure. The parameters of the void network are constrained by the cosmic microwave background (CMB) fluctuations and by the abundance and size of the large empty regions seen in local galaxy redshift surveys. The model may account for the excess of CMB temperature anisotropy power measured on cluster scales by the Cosmic Background Imager (CBI). We show that the $z = 0$ cluster mass function differs little from predictions for a standard Λ CDM cosmology with the same σ_8 , but that the evolution of the mass function at $z \sim 1$ is slower than in a gaussian model. Because massive clusters form much earlier in the "void" scenario, we show that future integrated number counts of SZ sources and simple statistics of strong lensing will provide additional constraints on this non-gaussian model.

Key words: cosmology: theory – large-scale structure of the Universe – cosmic microwave background galaxies: clusters: general

1 INTRODUCTION

The emergence of the Λ CDM scenario as the standard model for both the evolution of the cosmological background and the development of large-scale structure has recently received dramatic confirmation from the *WMAP* microwave background experiment (Spergel et al. 2003) and from the large-scale distribution of galaxies (Peacock et al. 2001; Tegmark et al. 2003a).

In this picture of minimal complexity, adiabatic gaussian fluctuations in the energy density with scale-invariant power law power spectrum generated in the early Universe are stretched during inflation to astrophysically relevant scales. Gravitational instability is then responsible for amplifying the resulting overdensities and for the collapse of structure. In hierarchical models like cold dark matter (CDM), small objects collapse first and the more massive clusters form relatively recently. Although successful in many aspects, the ability of the model to reproduce the mass function of satellites of the Milky-Way (Tully et al. 2002; Stoehr et al. 2002), the rotation curves of LSB galax-

ies (McGaugh et al. 2003), or the bulk properties of the stellar populations of massive ellipticals (Peebles 2001) is still uncertain, even if recent hints towards tilt and/or running of the primordial spectrum index (Peiris et al. 2003) might help resolve some of the discrepancy on small scales.

On larger scales, the voids seen in the nearby galaxy distribution (El-Ad & Piran 2000; Peebles 2001; Hoyle & Vogeley 2002) or the still controversial large-scale features (Broadhurst et al. 1990; Percival et al. 2001; Frith et al. 2003) justify the development of more complex, non-gaussian scenarios where linear, two-point predictions are in agreement with observations of the CMB, with the hope that simulations of galaxy formation in different environments and of the Lyman- α forest will agree with observations at least at the level of Λ CDM (Kauffmann et al. 1999; Springel et al. 2001; Mathis & White 2002; Croft et al. 2002, see also van den Bosch et al. 2003).

We consider one such alternative to the concordance model, where primordial bubbles of true vacuum that formed in a first-order phase transition during inflation can survive to the present day and result in cosmological voids (La 1991; Liddle & Wands 1991; Occhionero et al. 1997; Occhionero & Amendola 1994). This model is typically im-

* Email: hxm@astro.ox.ac.uk

plemented in the context of so-called 'extended inflation' (La & Steinhardt 1989). With reasonable values for the distribution of voids, Griffiths et al. (2003, hereafter G03) (see also Baccigalupi et al. 1997; Baccigalupi & Perrotta 2000) have shown that the angular power spectrum of CMB temperature anisotropies in this primordial void model with Λ CDM-type cosmological parameters fits the observations at $l \lesssim 800$. The signature of voids emerges at $l \gtrsim 1000$ and, if $\sigma_8 = 0.9$, could account for the excess power seen by the Cosmic Background Imager (CBI) on cluster scales ($l \sim 2500$) if it is not due to an underestimate of the Sunyaev-Zel'dovich (SZ) (see fig. 3 of G03). While viable in terms of the temperature angular power spectrum, we note that Corasaniti et al. (2001) derive constraints on the underdensity and volume fraction of voids at recombination from the COBE-DMR three-point correlation function and that Baccigalupi & Perrotta (2000) predict non-gaussian features in the CMB temperature fluctuations that have yet to be tested against high-resolution maps. On galaxy scales, G03 note that their void model may naturally account for the large underdensities seen in the local galaxy distribution which may be difficult to explain within the gaussian Λ CDM paradigm (Peebles 2001; Gottloeber et al. 2003, however see Mathis & White 2002), and use the observed typical local void radii and filling fractions to set two of the free parameters of their void model.

To assess this void model from another direction which could lead to simpler observational constraints, we simulate large-scale structure formation using collisionless dark matter simulations of a network of compensated voids embedded in a Λ CDM cosmology. Due to the strong non-gaussianity, using concordance values for Ω_0, σ_8 results in a present-day cluster mass function (MF) that departs from the gaussian case. Non-linear structures develop much earlier in the void model, the result both of gravitational instability in the compensating dark matter shells surrounding the voids and of the large-scale motions triggered by the nonlinear evolution of the voids + shells systems. Integrating the cluster evolution up to $z \sim 5$, we show that simple number counts of SZ sources and optical depth to strong lensing are enhanced with respect to the Λ CDM scenario and that such observations may easily rule out the void model. Note that Amendola & Borgani (1994) have compared the angular two-point correlation function and the scaling of higher-order moments of a series of models with primordial voids to available observations of galaxy clustering. Their approach was however semi-analytical and lacked dynamical evolution of the structures.

This paper is organised as follows. In Section 2, we recall the parameters of the void distribution and the approximations we make, the same as G03. In Section 3, we discuss the set-up of the initial conditions, make simple checks and present results at $z = 0$. We deal with the high- z cluster evolution in Section 4, and motivate our choice of observables. We conclude in Section 5.

2 PHENOMENOLOGICAL MODEL

2.1 Parameters

We take the parameters of the fiducial void model of G03. The background is a flat, dark energy dominated cosmology

with $h=0.7, \Omega_0 = 0.3, \Lambda_0 = 0.7$ and we normalize the amplitude of the mass fluctuations so that $\sigma_8 = 0.9$. This set of parameters is close to the best-fit obtained from the combined *WMAP* + SDSS data (Tegmark et al. 2003b). We assume that fluctuations of the field driving inflation produce the usual gaussian adiabatic scale invariant perturbations, filtered as they reenter the horizon by a CDM transfer function. Variants of extended inflation predict that the first bubbles to nucleate during the phase transition can reach cosmological sizes at recombination. The cumulative number density of the voids is taken to be :

$$N_V(> r) = A r^{-\alpha} \quad (1)$$

where r is the physical void radius, A a normalisation constant adjusted to match the present-day filling fraction of voids seen in galaxy redshift surveys, and the exponent α is related to the gravitational coupling ω of the inflaton if extended inflation can be described with a Brans-Dicke formulation :

$$\alpha = 3 + \frac{4}{\omega + 1/2} \quad (2)$$

Solar system experiments require $\omega > 3500$ (Will 2001) and we will take here $\alpha = 3$. The lower and upper cutoffs in the void radii $r_{\min, \max}$ are chosen to agree with redshift surveys. Plionis & Basilakos (2002) and Hoyle & Vogeley (2002) measured the typical size of voids in the *PSCz* and *UZC* surveys and found that up to half of the volume of the universe is underdense with $\delta\rho_{\text{gal}}/\rho_{\text{gal}} \lesssim -0.9$. The void radii they obtain range from 10 to 30 h^{-1} Mpc with an average of $\sim 15 h^{-1}$ Mpc. Following G03 we assume $r_{\min, \max} = 10, 25 h^{-1}$ Mpc. (The contribution to the CMB temperature anisotropy angular power spectrum on CBI scales is mostly due to the voids with the largest radii; an analysis constraining r_{\max} using the CMB data alone is in progress.) Examples of physical motivations for the lower and upper cutoffs are that (1) on subhorizon scales, matter flows relativistically back into the voids after inflation during radiation domination, and suppresses the growth of small voids and that (2) the tunnelling probability of inflationary bubbles is modulated through the coupling to another field, resulting in a maximum radius. (See Occhionero et al. 1997 for a model of extended inflation involving two scalar fields and which gives a lower cutoff.) Last, we take an observed $z = 0$ void filling fraction of $f_{\text{voids}} = 40\%$.

2.2 Approximations

In this section, we briefly review the assumed profiles and spatial distribution of the voids.

We neglect the contribution of baryons as our purpose is to obtain statistics for massive clusters, where the dynamics is controlled by the dark matter. As the CDM becomes non relativistic early in the expansion, it is expected to travel only minimally into the voids which reenter the horizon later and are of interest for structure formation. On the other hand, due to the tight coupling to photons, baryons will fill in voids which are within the horizon before decoupling at the adiabatic sound speed (Liddle & Wands 1991), before gravitation takes over from radiation pressure. If at some point the mass of baryons inside the voids reaches a substantial fraction of the mass of the shell, the growth of the

void radius will be slower than expected for a fully empty, compensated region. We simply mention that the precise dynamics of void filling by the baryons is complex and needs further study when comparing for instance the high-redshift distribution of voids with the clustering of the Lyman- α forest, and that the precise density profile of the voids depends on the physics of reheating and of the subsequent filling by baryons.

Smooth void density profiles have been considered in analytical work: rounded step functions (Hoffman et al. 1983; Martel & Wasserman 1990), exponentials (Hausman et al. 1983) or periodic functions (Baccigalupi 1998). However, with the exception of Regos & Geller (1991) who also use a smooth initial profile, numerical simulations of void evolution using particles often approximate voids as “top-hat” underdensities (Dubinski et al. 1993; White & Ostriker 1990; Robinson & Baker 2000, hereafter W90, R00). These authors do not consider any particular physical model, but rather use generic templates of single voids or void networks. Here, to follow G03 we suppose that the voids at decoupling are spherical “top-hat” underdensities with $\delta\rho_{\text{DM}}/\rho_{\text{DM}} = -1$ surrounded by a thin compensating shell of dark matter.

In an EdS cosmology, the shell density profile can be exactly derived from the self-similar solution of the evolution of a spherical underdensity (Bertschinger 1985, hereafter B85). We assume that all the matter swept up during the expansion of the void ends up in the compensating shell around it. This behaviour results naturally from the expansion of an underdense region in an EdS cosmology (where the thickness of the shell is very slowly growing, see B85), a very good approximation to Λ CDM when we start the simulations. Recall that G03 assume for simplicity an EdS cosmology to compute the void contribution to the angular power spectrum of the CMB anisotropies, and add the result to the power spectrum of the concordance Λ CDM model employed here. This makes sense, because (1) most of this contribution comes from voids close to the last scattering surface (LSS) where Λ CDM is similar to EdS and (2) the contribution to the power spectrum varies smoothly with l , reducing the small impact of the correction for angular diameter distance even further.

As in G03 we ensure that the voids do not initially overlap, although there seems to be no physical motivation for such a restriction. In practice, given the starting redshift we choose, our results depend very weakly on this hypothesis. Finally, the positions of centers of the voids are initially uncorrelated.

3 SIMULATING THE VOID NETWORK

3.1 Initial conditions

We focus on two collisionless simulations of side $200 h^{-1}$ Mpc using 128^3 particles, carried out with the publicly available N-body tree-SPH code GADGET without hydrodynamics¹. The first simulation, called G , is a gaussian Λ CDM model with the above parameters, the second, V , is the Λ CDM + voids non-gaussian fiducial model of G03. Except for the total initial displacement field, all simulation

parameters are similar in the two cases. The simulations employ a Plummer softening length $\epsilon = 0.08 h^{-1}$ Mpc which was kept fixed throughout in comoving coordinates.

The size of the box is a compromise between the necessity of having enough primordial voids covering the whole radius range at $z = 0$, $[10\ 25] h^{-1}$ Mpc, and the mass resolution. (The comoving radius range is $[3\ 6.3] h^{-1}$ Mpc at the starting redshift z_{init} .) Even independently of the halo resolving power, $N_{\text{parts}} = 128^3$ is a stringent lower limit to the number of particles as simulations need to (1) propagate information about the smallest voids present at the starting redshift, (2) have sufficient initial power in the cosmological displacement field with respect to the power due to shot noise as one approaches the Nyquist frequency of the particles not to alter significantly the formation of the smallest haloes one can resolve and (3) ensure that 2-body scattering effects are not important. While condition (1) is easy to verify with our number of particles, (2) and (3) are a little more complex, as these issues can be amplified because we use non-gaussian initial conditions for V . In addition, because of the strong primordial non-gaussianity, the formation of structure may also depend on the type of the initial distribution of particles which is employed before applying the initial displacement field, *i.e.* whether one starts from a grid, a random (Poissonian), or a glass (Baugh et al. 1995; White 1996) distribution. In the case of a grid, shot noise is minimal but the mesh introduces a characteristic scale and three preferred directions. A fully random, Poissonian distribution has no preferred direction but shot noise is significant. As a compromise between the two, we have used a glass distribution, which does not have any preferred direction, but with intrinsic power spectrum rising as $P(k) \propto k^4$. We find haloes with a friends-of-friends algorithm (Davis et al. 1985) with a $z = 0$ linking length $b\bar{l} = 0.164$ times the mean interparticle separation \bar{l} . At redshifts $z = 1, 2$ and 3 , we have used the usual EdS linking length parameter $\bar{b} = 0.2$ since Λ CDM behaves as an EdS cosmology at these epochs (this corresponds well to the $b \propto (\Delta_c/\Omega)^{-1/3}$ scaling proposed by Eke et al. 1996, see also Jenkins et al. 2001). We keep only the groups with more than 10 particles and the minimum total halo mass we can resolve is $M_{\text{min}} = 3.16 \times 10^{12} h^{-1} M_{\odot}$. To address the issue of the choice of the initial distribution, we have checked that using a grid rather than glass for the initial distribution of particles in V does not change the $z = 0$ MF of dark matter haloes. To deal with the impact of the level of shot noise compared to the amplitude of the initial cosmological perturbations, we verify below that the simulated $z = 0$ MF of G matches analytical results (this is sufficient as we will show that the initial power spectrum of G is smaller than that of V over all simulated scales). Finally, we have found the $z = 0$ number of dark matter haloes of V to depend on the starting redshift when using only $N_{\text{parts}} = 64^3$ particles, a signature of unphysical resolution effects, but to have converged with $N_{\text{parts}} = 128^3$ particles.

In G , the initial displacement field $\vec{\mathbf{d}}$ is given by the usual Zel'dovich approximation applied to the CDM power spectrum, normalised to a present $\sigma_8 = 0.9$. We compute $\vec{\mathbf{d}}$ on a 128^3 mesh. In V , it is the *same* $\vec{\mathbf{d}}$ for particles outside any primordial void and the displacement predicted by the similarity solution of B85 taken in the EdS regime ($r \propto t^{4/5}$ where r is the physical void radius and t the time) for all

¹ <http://www.mpa-garching.mpg.de/~volker/gadget/index.html>

particles that fall within a primordial void. Given the assumptions of paragraph 2.2, we put all particles falling in a void at its radius, and assign them the radial velocity of the expanding shell, following W90. In that sense, our V simulation would be close to that of a “spontaneous creation” of voids at z_{init} .

To follow G03, we use the similarity solution of an EdS universe (in particular the EdS time elapsed from z_{init} to $z = 0$) to compute the initial radii and shell velocities of the voids, although we run the simulations with a Λ CDM background. In doing so, we neglect differences expected with respect to EdS in the initial radii if voids were scaled back from $z = 0$ using a theoretical solution for a Λ CDM cosmology. However, we verify below that this enables simulations to correctly reproduce single $25 h^{-1}$ Mpc radius voids at $z = 0$. Furthermore, the similarity scaling between void radius and shell velocity remains strictly valid at z_{init} if it is high enough as EdS is then a very good approximation to Λ CDM (see B85).

The starting redshift for simulations of cosmological models with gaussian initial conditions is usually set by requiring the maximum particle displacement to be ~ 30 percent of the mean interparticle distance. An upper limit on z_{init} results from condition (1) on N_{parts} and translates the lower limit on the amplitude of the power spectrum of the initial perturbations. To choose z_{init} for their simulations of a non-gaussian model with primordial voids, R00 ensure that $\Delta^2 < 0.15$ at the Nyquist frequency of the particles and that no shell crossing occurs when initially displacing the particles. This is feasible as they compute the displacement for all their particles only from the Zel’dovich scheme applied to a linear density field. Their density field is the superposition of a gaussian field and a distribution of mildly underdense spherical regions with $\delta_{\text{void}} \sim 0.1$. Because we start our simulations with compensated empty voids, we immediately probe the non-linear regime on void scales. As a consequence, the MF of haloes that we obtain at $z = 0$ in the void model could depend on z_{init} : it is possible that some dark matter haloes that our simulation can resolve have formed before z_{init} by fragmentation of the void shells, and starting at z_{init} could ignore them. Therefore we conservatively start the simulations soon after decoupling with a high $z_{\text{init}} = 1000$, still satisfying condition (1). We have checked that the $z = 0$ halo mass function in V obtained from starting at $z_{\text{init}} = 1000$ is similar to that obtained from starting at $z_{\text{init}} = 3000$ (this is not true for a simulation of V with only $N_{\text{parts}} = 64^3$ particles). Independently of the shape of the one-point PDF of the initial overdensity field, a worry from such a high starting redshift is that numerical integration of the equations of motion might suppress the growth of small-scale modes (see the introduction of Scoccimarro 1998). Again, we use below the $z = 0$ halo MF of G to check that this does not affect our conclusions.

The initial gravitational potential $\Phi_{\text{tot}}(\vec{x})$ that we construct in the simulations can be linked to CMB observations. On void scales in the simulation V , like the overdensity field, Φ_{tot} will deviate from a realisation of a gaussian random field. As an example, Komatsu et al. (2003) look for a signature of non-gaussianity in the *WMAP* CMB temperature fluctuations maps using variants of the bispectrum and Minkowski functionals. They then constrain the relative contribution f_{nl}^2 of second-order deviations from a gaussian field

expected in single-field inflation models (e.g. Gangui et al. 1994; Verde et al. 2000) to the standard deviation of the gravitational potential but on a scale larger than the typical size the voids studied here would have on the LSS. Nevertheless, analysis of non-gaussianity on smaller scales will be possible soon with interferometric maps, and further constraints on the fiducial Λ CDM + voids model will result from comparisons with the theoretical bispectrum obtained in simulated maps of CMB temperature fluctuations.

Here we adopt a simpler approach to the non-gaussian contribution to the gravitational potential and estimate the relative amplitude of the gravitational potential energy of the gaussian component with respect to the total energy in the compensated voids. All energies are computed in proper coordinates; note that the total (kinetic and gravitational) energy of a compensated void, including the shell, is always positive (see B85). Recall also that in an EdS universe W is constant if the growth of the fluctuations is linear. We note E_{v} the total energy of the network of voids and shells in the V simulation and W_{g} the total gravitational potential energy of the gaussian density fluctuations as realised in the G (or V) simulation. At $z_{\text{init}} = 1000$, we obtain analytically $E_{\text{v}} = 7.09 \times 10^{22}$ while $W_{\text{g}} = -7.79 \times 10^{22} h^{-1} M_{\odot} \text{ km}^2 \text{ s}^{-2}$. In the remainder of this section, we will implicitly assume this unit when quoting energies.

Our analytical estimates show that at the starting redshift, the energy due to the voids is similar to that of gravitational potential of the gaussian density perturbations. In addition, the probability distribution function of the gravitational potential of a network of compensated voids over a homogeneous background is not gaussian (it is strongly positively skewed). As a result, we expect f_{nl}^2 in the expansion of Komatsu et al. (2003) to reach values of order unity on the angular scale of the voids, but a precise calculation also separating kinetic and gravitational energy of the voids+shells network is left for future work.

In practice, because of shot noise and of transients from the Zel’dovich approximation, it is not easy to obtain a precise value for the potential energy at high redshift directly from the particle distribution in the simulations (irrespective of a possible primordial non-gaussianity). We have checked that at $z \sim 10$ the predicted and measured values of W_{g} agree within 20 percent.

At $z = 0$, using the EdS similarity solution for the evolution of the network of voids and shells in a Λ CDM background, we obtain $E_{\text{v}} = 4.45 \times 10^{22}$, and *assuming* the Λ CDM linear growth of the gaussian density fluctuations to be valid up to the Nyquist frequency of the particles we get $W_{\text{g}} = -6.07 \times 10^{22}$. With this hypothesis of linearity in our whole box, the energy of the voids and shells drops at late times to 70 percent of the potential energy. In other words, from z_{init} to $z = 0$ the analytical E_{v} decreases by more than the factor $D_{\text{lin},\Lambda\text{CDM}}/D_{\text{lin,EdS}}(z_{\text{init}} \rightarrow 0) < 1$ describing the evolution of W_{g} .

Directly in the simulations, we measure the total gravitational potential $W_{\text{sim}} = -2.22 \times 10^{23}$ in V and -1.85×10^{23} in G . The excess factor of 2-3 between measurements and analytical predictions for W_{sim} in G is due to the non-linear evolution of the density field. The lower W_{sim} measured in V compared to G can be a consequence of the slightly larger number of haloes that we find in V at $z = 0$. On the basis of the predicted E_{v} at $z = 0$, one would expect W_{sim} to be

Figure 1. Final particle distribution in a Λ CDM background simulation (without the cosmological gaussian perturbations) of a $25 h^{-1}$ Mpc - radius void centered on a $100 h^{-1}$ Mpc box. The slice shown has thickness $10 h^{-1}$ Mpc. The radii of the inner and outer solid circles are respectively the comoving input at z_{init} ($6.3 h^{-1}$ Mpc) and $25 h^{-1}$ Mpc.

higher in V than in G . This is not measured, however, because as seen in G non-linear effects determine the late-time value of W_{sim} .

For completeness, the total kinetic energy measured in the simulations right after setting the initial conditions is $K_{\text{tot}} = 1.44 \times 10^{16}$ and 1.60×10^{14} in the V and G simulations respectively ($K_{\text{tot}} = 1.19 \times 10^{23}$ and 1.02×10^{23} at $z=0$). The peculiar velocities assigned to dark matter particles constituting the void-compensating shells is responsible for the large excess of initial kinetic energy in V . At late times, this excess is washed out in the dominant contribution of the particles of virialized haloes.

3.2 Consistency checks

To check the effect of periodic boundary conditions, we simulate with GADGET the growth from z_{init} of a single void with final radius $25 h^{-1}$ Mpc centered on a $100 h^{-1}$ Mpc box without the gaussian part of the displacement field, in a EdS universe. We use the EdS similarity solution to scale back to z_{init} . At $z = 0$, we find that the total mass enclosed inside 99 % (98 %) of the inner shell radius of $25 h^{-1}$ Mpc is 9 % (3%) of that expected in a similar volume with mean density. The same test is repeated with the scaling method described above for simulations in a Λ CDM background and we find a similar “leaking” mass fraction, see Fig. 1. In both cases a large fraction this remaining mass is contributed by particles of clusters formed on the shell. Down to $z = 0$, the particle distribution remains smooth beyond a $27 h^{-1}$ Mpc radius.

We verified that the $z = 0$ halo MF of the G simulation gives results in agreement with the fitting formula of Jenkins et al. (2001, hereafter J01) and that it is robust against changes in z_{init} . (Using $N_{\text{parts}} = 32^3$ rather than $N_{\text{parts}} = 64^3$ or 128^3 for the G simulation results in an excess of low mass haloes if $z_{\text{init}} = 1000$, and using $N_{\text{parts}} = 64^3$ rather than 128^3 for the V simulation leads to a redshift dependence of the MF: a factor 3 more massive haloes than for $N_{\text{parts}} = 64^3$ and $z_{\text{init}} = 100$).

The validity of using the Zel’dovich approximation when setting up the initial conditions is checked on large scales by the growth of the largest modes of the simulation, in agreement with linear theory down to $z = 0$. We have finally performed two other simulations of the void model, changing both the gaussian random perturbation field and the positions of the voids, and found results very similar to those for V .

3.3 Results at $z = 0$

Fig. 2 shows the projected (2D) density of two slices of side $200 h^{-1}$ Mpc and thickness $20 h^{-1}$ Mpc cut at the same position through the V and G simulations (left and right panels respectively). Recall that the two simulations use the

same initial gaussian displacement field, which in the case of V is combined with the displacement due to the primordial voids. The grey scale is the same in the two cases. Note the voids in the slice through V , apparent immediately below the centre of the picture and at the middle of the upper frame, together with a void network developing at the centre left.

Fig. 3 gives the initial and $z = 0$ real-space overdensity power spectra (dotted and solid lines for the G and V simulations respectively). Also shown are the power spectra of the unperturbed glass initial particle distribution (dash-triple dotted line), and of the initial conditions for the G and V simulations (dashed and dash-dotted lines). All spectra have been divided by the linear growth factor for clarity. The diamonds with associated error bars show the real-space galaxy power spectrum as measured by Tegmark et al. (2003a) from the DR1 of the SDSS survey.

The imprint of the voids is significant at z_{init} at $k \gtrsim 0.1 h \text{ Mpc}^{-1}$, as is clear when comparing the dash-dotted and dashed lines. At $z = 0$, non-linear power is larger in the void model than in the Λ CDM model, and departure from the evolved Λ CDM power spectrum occurs as early as $k = 0.1 h \text{ Mpc}^{-1}$. Of course a precise comparison between the V power spectrum and the data would need to correct for bias, a quantity that might show a different behaviour in the Λ CDM + voids model than in Λ CDM. If a precise assessment of galaxy bias falls beyond the scope of this work, we note that at $k = 0.25 h \text{ Mpc}^{-1}$, the dark matter bias of the Λ CDM + voids model with respect to the Λ CDM model is not more than 1.15. At the same scale, the bias of the evolved dark matter density field of the Λ CDM + voids model with respect to the galaxy distribution reaches 1.3, a high but plausible value.

The main panel of Fig. 4 compares the halo MF measured at $z = 3, 2, 1$ and 0 from left to right in the G and V simulations (dotted and solid lines respectively) to the data and to the fitting formula of J01 calculated for the parameters of the gaussian Λ CDM model we have simulated (dash-dotted lines). While the G simulation agrees well with J01, there are systematically more haloes in the V simulation at $z = 0$, for mass thresholds $M_{\text{min}} \leq 5 \times 10^{14} h^{-1} M_{\odot}$. The excess is a factor 1.5 in the abundance. For higher mass thresholds, the abundance is similar in the two models. This is more clearly seen in the insert in Fig. 4, which gives the differential halo MF measured around $2 \times 10^{14} h^{-1} M_{\odot}$. The excess of the non-gaussian model is apparent at all mass scales smaller than $3 \times 10^{14} h^{-1} M_{\odot}$. For higher masses the two curves are identical. We find one halo with $M_{\text{tot}} > 10^{15} h^{-1} M_{\odot}$ in both the G and V simulations. (Recall that the gaussian part of the initial overdensity field is normalised to the same present-day $\sigma_8 = 0.9$).

Bahcall & Cen (1993) give $N_{>M} = 2 \pm 1 \times 10^{-6} h^3 \text{ Mpc}^{-3}$ at $M = 4 \times 10^{14} h^{-1} M_{\odot}$. Even assuming their uncertainty factor of 1.3 in the mass of rich clusters, this normalisation falls significantly below both our V and G mass functions. The present-day MF of the V simulation is therefore only marginally consistent with this normalisation, but the level of disagreement is the same as that of a Λ CDM model with concordance cosmological parameters and $\sigma_8 = 0.9$. Diamonds with error bars on Fig. 4 show the more recent data of Bahcall et al. (2003); Bahcall & Bode (2003) who constrain the amplitude of mass fluctuations using the “optical” mass function of clusters selected from

Figure 2. Left and right panels: projected 3D density at $z = 0$ in slices cut at the same position through the Λ CDM + voids and gaussian (Λ CDM) simulations respectively. The side and thickness are 200 and $20 h^{-1}$ Mpc. The *gaussian* initial displacement field is the same in both simulations. The grey scale is the same for the two panels. Note on the left panel the voids right below the centre of the picture, at the middle of the upper frame, and a void network developing a “honeycomb” structure at the centre left.

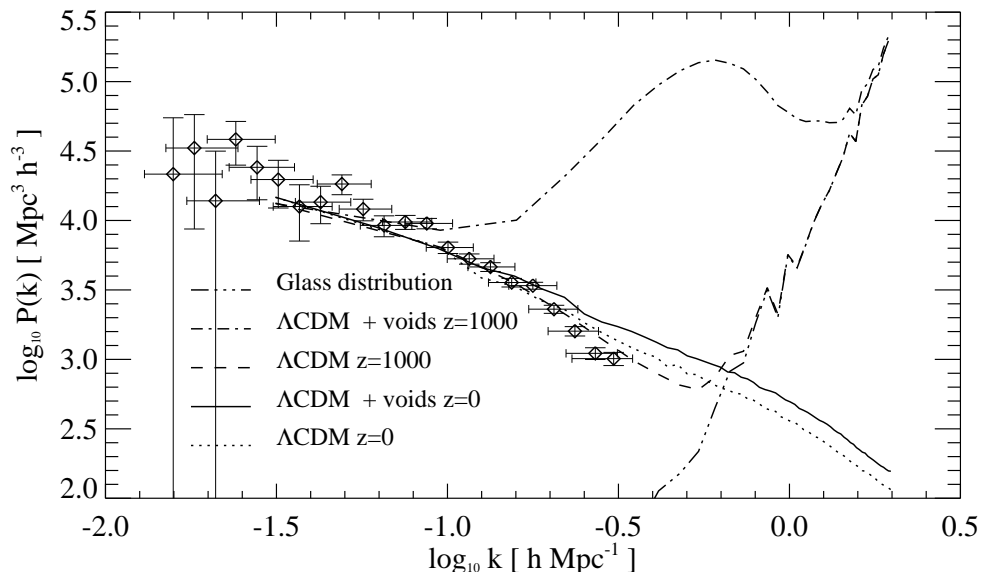


Figure 3. Real-space matter overdensity power spectrum at $z = 0$ of the gaussian (Λ CDM) and non-gaussian (Λ CDM + voids) simulations : dotted and solid lines respectively. The dashed and dash-dotted lines show the same respective quantities at $z = 1000$, after division by the linear growth factor for clarity. The dash-triple dotted line is the power spectrum of the raw glass file, for comparison. Note the signature of the voids in the initial conditions at $k \gtrsim 0.1 h \text{ Mpc}^{-1}$ and the stronger $z = 0$ non-linear power in the void model. Diamonds with error bars show the real-space galaxy power spectrum from Tegmark et al. (2003a) (a more direct comparison between the Λ CDM + voids simulation and the data would need a detailed model for galaxy bias).

the SDSS EDR. They find a normalisation similar to that of Bahcall & Cen (1993), with best-fit values $\sigma_8 = 0.9$ and $\Omega_0 = 0.19$. From a combination of X-ray and optical observations, Vikhlinin et al. (2003); Voevodkin & Vikhlinin (2003) derive constraints on the cosmological parameters Ω_0 , Λ_0 from the evolution of the cluster baryon mass fraction up to $z \sim 0.5$, requiring σ_8 to be set by the observed amplitude of the $z = 0$ baryon mass function. Their $z = 0$ and $0.4 < z < 0.8$ total mass functions for massive clusters are reported with triangles and squares respectively on Fig. 4 (we have omitted their error bars for clarity, and corrected for a weak mass dependence of the cluster baryon fraction, see Vikhlinin et al. 2003). The $z = 0$ mass function of Vikhlinin et al. (2003) agrees with Bahcall et al. (2003). At high redshift, the observed mass function has a lower normalisation than both the G and V $z = 1$ mass functions, a repeat of the $z = 0$ differences.

In fact, it is clear from Fig. 4 that the difference of the fiducial model of G03 with respect to Λ CDM is much more significant in the intermediate and high- z mass functions. Unfortunately, measurements of the cluster mass function at high redshift $z \gtrsim 1$ from X-ray observations are subject to uncertainties in, for instance, the redshift evolution of the L-T and M-T cluster scaling relations (see however

Voevodkin & Vikhlinin 2003). In the following section we will consequently use integrated SZ cluster counts and the abundance of giant arcs to probe the signature of the void model, rather than the cluster mass function.

We conclude this section with two additional tests at $z = 0$, first changing the parameters of the void model and then comparing with two gaussian models.

We have simulated another primordial void model V' of the same type as V but with a much steeper spectrum for the distribution of initial void radii (using $R_{\text{min,max}} = 10, 40 h^{-1}$ Mpc, $\alpha = 6$, $f_{\text{voids}} = 40\%$). G03 show that this model also agrees reasonably well with high and low- l measurements of the angular power spectrum of the CMB temperature fluctuations. The V' $z = 0$ cluster MF shows a large excess compared to the V MF (an order of magnitude more massive clusters and $\sigma_8 \sim 2$), so that this set of void parameters is directly ruled out.

Second, it is necessary to check the impact of non-gaussianity by comparing to a model with gaussian initial conditions but with an initial power spectrum similar to that measured in the void model right after setting the initial conditions. For this purpose, we have simulated two gaussian models V_1 and V_2 with the same cosmology and starting redshift as V and G but taking as initial power spectrum the

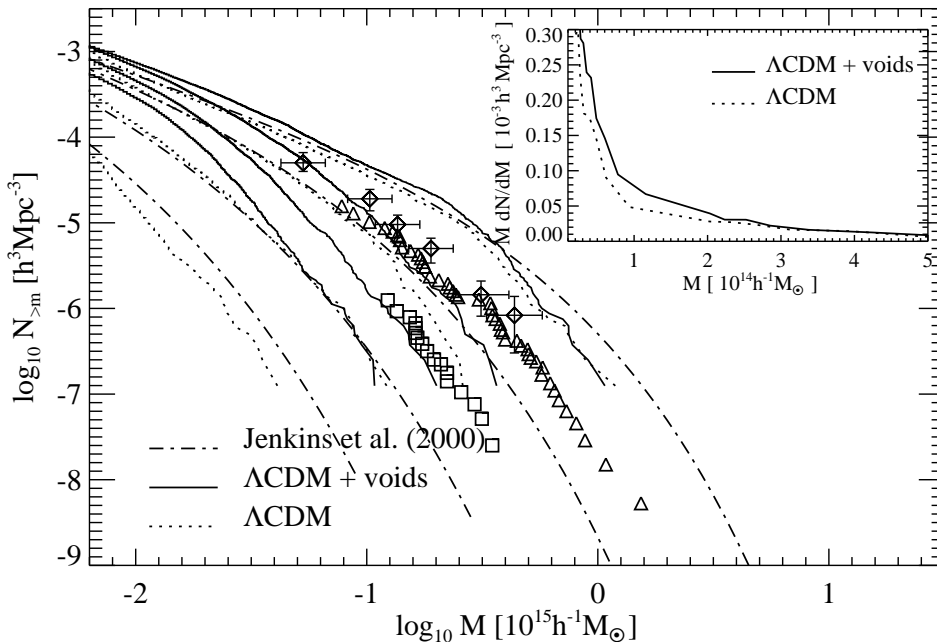


Figure 4. Main panel: mass functions of the gaussian (Λ CDM) and non-gaussian (Λ CDM + voids) simulations: dashed and solid lines respectively, measured at $z = 3, 2, 1$ and 0 from left to right. The dash-dotted line is the fitting formula of J01 to Λ CDM. The diamonds with error bars show the “optical” mass function that Bahcall et al. (2003) obtain using the EDR of the SDSS. The triangles and squares give the cluster total mass functions at $z = 0$ and $0.4 < z < 0.8$ respectively. They have been derived from the cluster baryon mass function constructed by Vikhlinin et al. (2003); Voevodkin & Vikhlinin (2003) using a combination of optical and X-ray data (their error bars are omitted for clarity). Insert: differential mass functions $dN/d \ln M$ of the gaussian (Λ CDM) and non-gaussian (Λ CDM + voids) simulations: dashed and solid lines respectively, measured at $z = 0$ up to $5 \times 10^{14} h^{-1} M_{\odot}$.

dash-dotted line $P_{\text{voids,init}}$ of Fig. 3. V_1 and V_2 correspond to two different normalisations of the input power spectrum: for V_1 we have taken $P_{\text{voids,init}}$ of Fig. 3 divided by the linear growth from $z = 1000$ to $z = 0$, while for V_2 we have normalised so that the simulation has $\sigma_8 = 0.9$ at $z = 0$ (the adopted normalisation for V_1 results in $\sigma_8 \sim 4$ at $z = 0$). We have found the $z = 0$ cluster mass function of V_1 to largely exceed that of V and G (there is a factor of 5 more haloes with masses $M_{\text{tot}} > 4 \times 10^{14} h^{-1} M_{\odot}$) and that of V_2 to be abruptly cut at masses $M_{\text{tot}} \sim 10^{14} h^{-1} M_{\odot}$. In addition, the matter power spectra measured at $z = 0$ in V_1 and V_2 retained the strong feature (“bump”) seen in the initial conditions at $k_{\text{void}} > 0.1 h \text{ Mpc}^{-1}$ as a step-like increase at k_{void} which was only little modified by the late-time non-linear evolution. This is clearly ruled out by the data. To summarise, the non-gaussianity of the primordial void model is necessary to approximately reproduce the $z = 0$ observed cluster mass functions and mass power spectra: employing the initial power spectrum of the void model in a gaussian primordial density field results in a large mismatch to the data. The large peculiar velocities of the compensating shells surrounding the voids and associated to the scale k_{void} are not realised in a gaussian model with same initial power spectrum as V . As a result, the pattern at k_{void} in the power spectrum is more stable and persists longer in our V_1 and V_2 tests than in V , where large velocities may dilute/broaden the feature. The particular shape of the power spectrum

resulting from the void network is not transposable to a gaussian initial probability function.

4 DERIVING OBSERVATIONAL CONSTRAINTS

In this Section, we make predictions for the thermal SZ effect and for simple statistics of strong lensing. We show that they differ substantially in the primordial void model from their values in a Λ CDM cosmology. We note here that other observables like the cosmic shear or the clustering of the Lyman- α forest could also bring out the presence of primordial voids, but they are more complex than the former and may be affected by biases due to the non-linear evolution of the power spectrum.

4.1 SZ source counts

We first estimate the counts expected from the detection of the cluster thermal SZ effect, up to $z = 5$. Kay et al. (2001) make detailed analytical predictions for the SZ number counts expected for the *Planck* satellite using large simulations of cluster formation in gaussian CDM cosmologies. We follow the same approach but with simplifying assumptions. We use 30 simulation outputs for G and V from $z = 0$ to $z \sim 5$. Each dump has a comoving size $200 h^{-1} \text{ Mpc}$ and

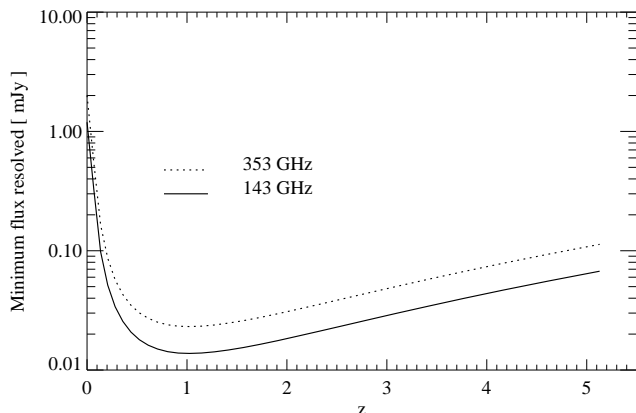


Figure 5. 143 and 353 GHz resolution limit for the cluster thermal SZ effect in the simulations as a function of redshift. The sensitivity of *Planck* to the SZ effect is of order 30 mJy (Bartelmann 2001), that of the planned Bonn-Berkeley *APEX - SZ* survey will reach 3 mJy at 150 GHz.

we find their DM halos above the minimum mass threshold M_{\min} . For simplicity we assume for each halo an isothermal profile for the gas (see, e.g., Barbosa et al. 1996) with total mass $M_{\text{gas}} = f_b \times M_{\text{tot}}$ where $f_b = 0.13$ is the cosmic baryon fraction. Taking the clusters to be point sources, we compute the magnitude of the flux change observed against the CMB at the *Planck* satellite frequencies 143 and 353 GHz, on both sides of the zero-point of the SZ thermal effect (217 GHz). Fig. 5 shows the minimum SZ flux that the simulations can resolve as a function of z . In the following, we show results for fluxes $S_\nu > 10$ mJy.

Fig. 6 gives the expected redshift distribution of SZ sources with $S_\nu > 10$ mJy in the Λ CDM + voids and Λ CDM models (solid and dotted, dashed and dash-dotted lines respectively), for 143 and 353 GHz. The curves have been fitted by polynomials in the relevant range. While there are virtually no sources with $S_{143, 353 \text{ GHz}} > 10$ mJy at $z \gtrsim 1.6$ ($z \gtrsim 2.1$) in G , the distribution of such objects in the void model is different. At 143 GHz, there are more sources in V at low redshift compared to G (a factor 1.3 in excess at $z = 0$, reaching more than 2 at $z = 1$), and the distribution of sources extends to $z = 2.6$ on the window shown. At $z > 4.3$, beyond the “dip”, the differential number counts of sources in V at 143 GHz again exceed 0.1, and keep increasing to $z \sim 5$ and earlier. At 353 GHz, SZ sources are intrinsically brighter and the differential number counts in V exceed 0.1 all the way to $z \sim 5$: the number counts decrease from $z = 0$ to $z \sim 3.4$, then increase to $z = 5$ and beyond. At $z = 0$, there is an excess by a factor 1.6 over the same V counts at 143 GHz, up to $z \sim 2$ where the ratio increases. At $z = 5$ the ratio between the 353 and 143 GHz differential counts in V is 2.5. With respect to G , the 353 GHz differential number counts in V are higher by 60 percent at $z = 0$, and by more than an order of magnitude at $z = 1.8$. At low redshift $z \sim 0$, the excess of sources in V compared to G is accounted for by the excess of clusters of mass $M_{\text{tot}} \sim 10^{14} h^{-1} M_\odot$ seen Fig. 4. The slower decrease in the number counts between $z = 0$ and $z = 3$ in V compared to G is the direct consequence of the slower late-

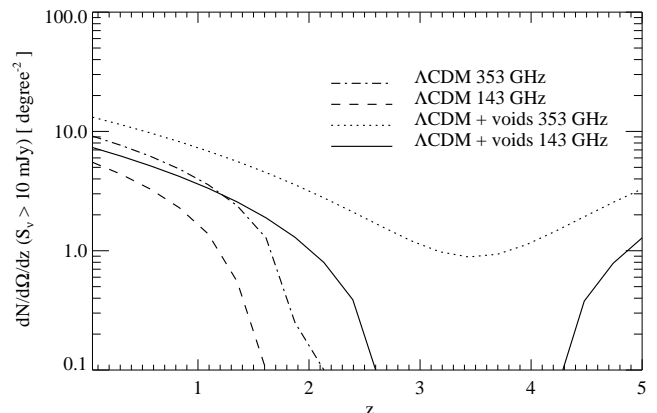


Figure 6. Redshift distribution of the sources with flux $S_{143, 353 \text{ GHz}} > 10$ mJy in the Λ CDM (dashed and dash-dotted lines) and Λ CDM + voids (solid and dotted lines) simulations.

time evolution of the cluster mass function in V compared to G . Finally, the increase in the differential number counts at $z \gtrsim 4$ in V is due to the flattening and decrease of the angular diameter distance at such redshifts in Λ CDM, together with the presence of massive, sufficiently hot haloes at these epochs in the void model.

In reality, there will be a residual number of sources with $S_{143, 353 \text{ GHz}} > 10$ mJy at $z > 5$ in the void model, as the results shown here provide only a lower limits to the counts, but the difference with respect to Λ CDM is already a factor of 2 at $z = 5$ and SZ surveys may therefore falsify the void model. The detection of sufficiently bright high-redshift SZ sources, on the other hand, would be a hint towards non-gaussianity.

To see how this conclusion varies with sensitivity, Fig. 7 gives the number counts of SZ sources expected (up to $z = 5$) in the Λ CDM (dashed and dash-dotted lines) and Λ CDM + voids (solid and dotted lines) models as a function of the flux threshold. Above a flux limit of 10 mJy, there are ~ 2 (~ 2.5) times more integrated counts at 143 (353) GHz in the Λ CDM + voids model compared to Λ CDM. The sensitivity of *Planck* to the SZ effect is of order 30 mJy (Bartelmann 2001) as shown by the vertical dash-triple dotted line, and the corresponding counts are enhanced by a factor 1.8 (2) at the two frequencies. For sources brighter than 100 mJy however, the excess in the number counts of sources in the primordial void model compared to Λ CDM drops to a factor 1.5 (1.25) at 143 (353) GHz, a ratio maybe too small to falsify the void model against Λ CDM with upcoming observations, even if a more detailed computation is needed at this level. Among many ground-based examples, the Bonn-Berkeley *APEX - SZ* survey² will cover 100 square degrees and is expected to reach a sensitivity of 3 mJy at 150 GHz. This 300-hour experiment will detect ~ 1000 clusters with mass $M_{\text{tot}} > 2 \times 10^{14} h^{-1} M_\odot$ up to $z = 2$ (assuming a Λ CDM model). It will provide strong constraints on non-gaussian models like primordial voids.

² <http://bolo.berkeley.edu/apexsz/>

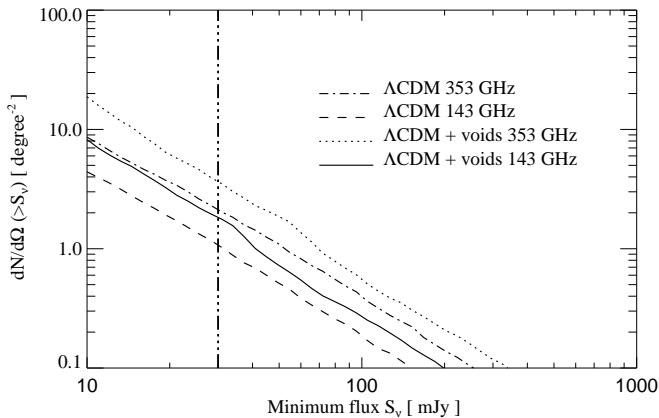


Figure 7. Number counts of SZ sources to $z = 5$ in the Λ CDM (dashed and dash-dotted lines) and Λ CDM + voids (solid and dotted lines) models as a function of the minimum flux $S_{\nu,\min}$ at 143 and 353 GHz. Note the enhancement (factor ~ 2.5) of the counts above $S_{\nu,\min} = 10$ mJy at 353 GHz in the model with primordial voids. The vertical line shows the sensitivity of *Planck*; at this level, number counts differ by a factor ~ 2 .

4.2 Strong lensing

The statistics of strong amplification of the images of background sources by massive concentrated structures is a powerful probe of the cosmological parameters (for example, Bartelmann et al. 1998). Clearly, they will also be directly affected by the primordial non-gaussianity considered here.

We assume that only the clusters that we can resolve in the simulations, ($M_{\text{tot}} \geq M_{\text{min}}$) produce strong lenses. We model the haloes with singular isothermal spheres (SIS) (Peacock 1982) and measure their velocity dispersions directly from the simulations. Perrotta et al. (2002) derive analytical predictions with NFW profiles for the differential amplification probability $P(A)$ and compare them to the predictions obtained with SIS profiles. For sources at $z_s = 4$ and 7, at $A \lesssim 3$ they find their Λ CDM model with NFW profiles to be more efficient than with SIS profiles. At $A \gtrsim 7$, SIS profiles yield the higher $P(A)$, but the probabilities for NFW and SIS profiles stay within a factor 3 of each other even at larger amplifications. We note here that we also neglect the impact of substructure and asphericity on the cross section for strong lensing, which may be significant but needs better understanding (see, e.g., Meneghetti et al. 2002).

Bartelmann et al. (1998) have computed the number of giant arcs expected on the whole sky for a series of gaussian CDM models and shown that only open CDM models could reproduce the total number of arcs seen in the EMSS sample. In particular, their open CDM model produced an order of magnitude more giant arcs than their Λ CDM model, assuming a redshift $z_s = 1$ for their sources. In a recent work, Wambsganss et al. (2003) study the effect of the redshift distribution of sources in the predicted number counts of giant arcs in a Λ CDM cosmology. They show that the lensing optical depth is a very steep function of the source redshift for $0.5 < z_s < 2.5$ and that it increases further for $z_s > 2.5$.

In fact, the order of magnitude discrepancy between the EMSS counts and the Λ CDM prediction is solved if one takes

a more extended distribution of sources to high redshifts. This is more realistic as a large fraction of the giant arcs Gladders et al. (2003) count in the Red-Sequence Cluster Survey (RCS) have high redshifts: $1.7 < z_{\text{arc}} < 4.9$. Putting a third of the sources at $z_s = 1.5$ rather than all sources at $z_s = 1$ increases the Λ CDM predicted counts by a factor 3, and putting 7 percent of the sources at $z_s > 3$ increases the counts by a factor of 7, bringing Λ CDM in agreement with the observations (Wambsganss et al. 2003).

Because the lensing optical depth is such a steep function of source redshift, one expects the large differences between the Λ CDM and the primordial voids models in the mass function of clusters at $z \sim 1 - 3$ (probing high source redshifts) to significantly affect the number counts of giant arcs, even without classifying the counts along arc (source) redshift. In the following, for simplicity, we compute our strong lensing statistics putting all our sources at high redshifts: $z_s = 3$ and then at $z_s = 5$. Detailed comparison to observations would require a more realistic model for the distribution of source redshifts, but our plots show the level of discrepancy expected between Λ CDM and Λ CDM + voids.

Fig. 8 shows the cumulative probability $P(A > A_{\text{min}})$ that a line of sight has an amplification larger than A_{min} in the Λ CDM and Λ CDM + voids cosmologies and for the two values of z_s . We take the strong lensing regime to be $A \gtrsim 2$. At $A_{\text{min}} \gtrsim 10$, the cumulative probability for strong lensing is a factor ~ 2 (~ 4) higher in the void model than in the Λ CDM case, for $z_s = 3$ (5). For sources at $z_s = 5$, we note that the enhancement is also larger than the possible bias due to our choice of an SIS rather than NFW halo profile. We conclude that the optical depth to strong lensing is increased in the Λ CDM + voids model compared to Λ CDM, and that the number counts of giant arcs may differ by up to a factor of 4, hence overpredicting the observations compared to Λ CDM. The optical depth to high-redshift galaxies will be increased by a factor of 4 in the void model, and the number counts of high-redshift giant arcs (with $z_{\text{arc}} \sim 5$) will be increased by more than a factor of 4 in the Λ CDM + voids model compared to the Λ CDM model, because the comoving density of bright ($M_* > 10^{10} h^{-1} M_\odot$) galaxies is also higher at $z \sim 5$ in the Λ CDM + voids model than in the Λ CDM model. (We verified this last point using a semi-analytical model for galaxy formation similar to that described in Mathis et al. 2002). If the density of the lensed population evolves similarly in the Λ CDM and the Λ CDM + voids models, then the mean redshift of the lenses will be shifted to higher values in V compared to G : Fig. 9 shows the redshift distribution of the total optical depth $d\tau/dz$ to strong lensing as defined in section 4.2 of Peacock (1999), for $z_s = 3$ and 5. The total optical depth τ is larger in the V than in the G simulation (note the factors ~ 2 and ~ 2.5 decrease between the V and G curves at $z_s = 3$ and 5 in Fig. 9).

Finally, we have assumed initially compensated voids surrounded by a thin shell growing as the underdensity expands in comoving coordinates. This large-scale configuration could *per se* constitute an efficient lens. However, Amendola et al. (1999) show that only voids with radius larger than $\sim 100 h^{-1}$ Mpc today induce weak gravitational lensing with a signal to noise ratio greater than unity in observables like color-dependent density magnification or aperture densitometry. Even for strong underdensities like

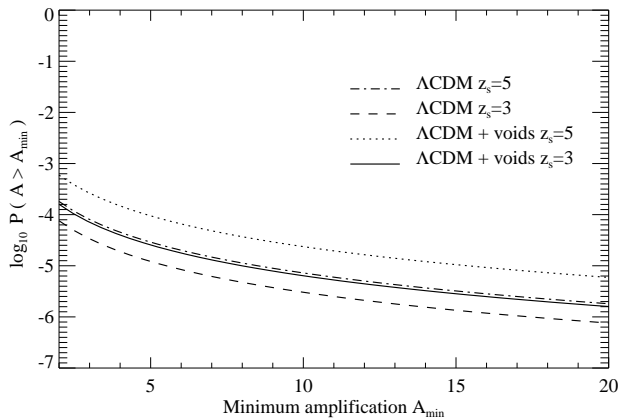


Figure 8. Probability $P(A)$ that a line of sight is magnified by $A > A_{\min}$ for the Λ CDM (dashed and dash-dotted) and Λ CDM + voids model (solid and dotted) for two source redshifts ($z_s = 3$ and 5 respectively). We suppose that the only lenses are the massive DM haloes with $M_{\text{tot}} > M_{\min} = 3.16 \times 10^{12} h^{-1} M_{\odot}$, modelled as singular isothermal spheres.

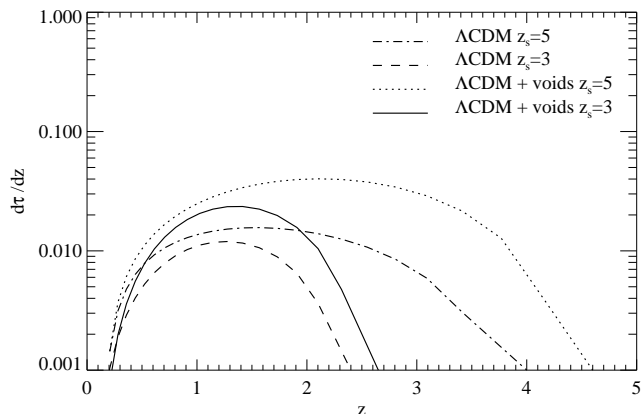


Figure 9. Redshift distribution of the optical depth to strong lensing $d\tau/dz$ contributed by our resolved haloes. The legend is the same as for Fig. 8. Note the ratio of ~ 2 to 2.5 between the primordial void model and the gaussian Λ CDM cosmology.

$\delta_{\text{void}} \sim -1$, none of these weak lensing techniques will be able to find a significant signature of the voids considered here.

5 CONCLUSIONS

We have simulated cluster formation in a physically plausible non-gaussian primordial void model where empty and fully compensated bubbles surviving from inflation together with the gaussian adiabatic CDM-type perturbations provide the seeds for the development of structure. This model shares the cosmological parameters of Λ CDM and possesses gaussian statistics on large scales while non-gaussianity only affects the one-point distribution on cluster scales. It is an attractive alternative to Λ CDM as it may explain the excess of CMB temperature anisotropy power at $l \sim 2500$

recently observed by CBI and as it could account for the large voids seen in the nearby galaxy surveys (Griffiths et al. 2003). While analysis of high-resolution CMB maps using higher-order moments will provide further constraints on primordial non-gaussianity, we have shown the evolution of the cluster mass function to be a strong constraint at low and intermediate redshifts.

At startup, the total energy of the network of voids and shells in our simulation is comparable to the potential energy of the gaussian fluctuations. Even if strong underdensities are present on Mpc scales very early on compared to Λ CDM, we have found that our $200 h^{-1}$ Mpc-side, 128^3 -particle simulations which start shortly after recombination can provide a reliable estimate for the cluster mass function of the non-gaussian model.

The power spectrum of the void model measured after setting the initial conditions shows a strong feature characteristic of the voids at $k \gtrsim 0.1 h \text{ Mpc}^{-1}$, which is then erased during the evolution by the non-gaussian initial conditions. The $z = 0$ matter power spectra of the Λ CDM + void model is close to that of the gaussian model, with little additional small-scale power at $k \gtrsim 0.5 h \text{ Mpc}^{-1}$. The $z = 0$ mass function gives a similar number of massive clusters ($M_{\text{tot}} > 4 \times 10^{14} h^{-1} M_{\odot}$) in the Λ CDM + voids model and in the concordance Λ CDM scenario. Our high cluster abundance compared to observations is a consequence of the *WMAP*+*SDSS* normalisation. The evolution of the cluster mass function up to $z \sim 3$ in the void scenario differs strongly from that of the Λ CDM model and is much more “efficient” than the sole $z = 0$ mass function in distinguishing between the two. The substantial evolution in the cluster baryon mass function seen by Vikhlinin et al. (2003) between $z = 0$ and $z \sim 0.5$ needs confirmation before we can falsify the non-gaussian model which has little late-time evolution.

In fact, better constraints on the void model are obtained from two other statistics at $z \gtrsim 1.5$. We have first shown that the integrated number counts of SZ sources is higher by a factor 2.5 (resp. 2) in the Λ CDM + voids model compared to the Λ CDM model, for 353 GHz flux greater than 10 mJy (resp. 30 mJy, the resolution of Planck). We have then used the optical depth to strong gravitational lensing as another possible discriminant between the primordial void model and Λ CDM. We have shown that the number counts of high-redshift, $z \gtrsim 3$ (resp. 5) arcs is expected to be more abundant by a factor of 2 (resp. 4) in the non-gaussian scenario, for the same underlying lensed population. Because the optical depth to strong lensing is a steep function of redshift, we expect the total number of giant arcs observed to be increased by a factor $\gtrsim 2$ in the Λ CDM + voids model compared to Λ CDM. As a result, the Λ CDM + void scenario overpredicts the number counts of giant arcs seen in the EMSS compared to the concordance Λ CDM.

An additional contribution to the CMB power spectrum at high ℓ will also be generated by the thermal SZ contribution from unresolved clusters. The joint limits on a non-gaussian contribution from clusters to the power spectrum, including the ROSAT/*WMAP* cross-correlation constraints (Diego et al. 2003) and the CBI and ACBAR experiments, will be presented elsewhere.

Not only do such simple tests give the opportunity to rule out a particular set of models, they also more generally

bring out simple constraints that have to be satisfied (e.g. with numerical simulations) as one proposes non-gaussian alternatives to the current paradigm.

ACKNOWLEDGEMENTS

We thank the referee for a number of remarks which significantly improved the manuscript. HM is supported by PPARC.

This paper has been typeset from a \TeX / \LaTeX file prepared by the author.

REFERENCES

- Amendola L., Borgani S., 1994, MNRAS, 266, 191
 Amendola L., Frieman J. A., Waga I., 1999, MNRAS, 309, 465
 Baccigalupi C., 1998, ApJ, 496, 615
 Baccigalupi C., Amendola L., Occhionero F., 1997, MNRAS, 288, 387
 Baccigalupi C., Perrotta F., 2000, MNRAS, 314, 1
 Bahcall N. A., Bode P., 2003, preprint, astro-ph/0212363
 Bahcall N. A., Cen R., 1993, ApJ, 407, L49
 Bahcall N. A., Dong F., Bode P., et al., 2003, ApJ, 585, 182
 Barbosa D., Bartlett J. G., Blanchard A., 1996, A&A, 314, 13
 Bartelmann M., 2001, A&A, 370, 754
 Bartelmann M., Huss A., Colberg J. M., Jenkins A., Pearce F. R., 1998, A&A, 330, 1
 Baugh C. M., Gaztanaga E., Efstathiou G., 1995, MNRAS, 274, 1049
 Bertschinger E., 1985, ApJS, 58, 1
 Broadhurst T. J., Ellis R. S., Koo D. C., Szalay A. S., 1990, Nature, 343, 726
 Corosani P. S., Amendola L., Occhionero F., 2001, MNRAS, 323, 677
 Croft R. A. C., Hernquist L., Springel V., Westover M., White M., 2002, ApJ, 580, 634
 Davis M., Efstathiou G., Frenk C. S., White S. D. M., 1985, ApJ, 292, 391
 Diego J. M., Silk J., Sliwa W., 2003, preprint, astro-ph/0302268
 Dubinski J., da Costa L. N., Goldwirth D. S., Lecar M., Piran T., 1993, ApJ, 410, 458
 Eke V. R., Cole S., Frenk C. S., 1996, MNRAS, 282, 263
 El-Ad H., Piran T., 2000, MNRAS, 313, 553
 Frith W. J., Buswell G. S., Fong R., Metcalfe N., Shanks T., 2003, preprint, astro-ph/0302331
 Gangui A., Lucchin F., Matarrese S., Mollerach S., 1994, ApJ, 430, 447
 Gladders M., Hoekstra H., Yee H. K. C., Hall P. B., Barrientos L. F., 2003, preprint, astro-ph/0303341
 Gottloeber S., Lokas E., Klypin A., Hoffman Y., 2003, MNRAS, 344, 715
 Griffiths L. M., Kunz M., Silk J., 2003, MNRAS, 339, 680
 Hausman M. A., Olson D. W., Roth B. D., 1983, ApJ, 270, 351
 Hoffman G. L., Salpeter E. E., Wasserman I., 1983, ApJ, 263, 527
 Hoyle F., Vogeley M. S., 2002, ApJ, 566, 641
 Jenkins A., Frenk C. S., White S. D. M., et al., 2001, MNRAS, 321, 372
 Kauffmann G., Colberg J. M., Diaferio A., White S. D. M., 1999, MNRAS, 303, 188
 Kay S. T., Liddle A. R., Thomas P. A., 2001, MNRAS, 325, 835
 Komatsu E., Kogut A., Nolta M. R., et al., 2003, preprint, astro-ph/0302223
 La D., 1991, PRD, 44, 1680
 La D., Steinhardt P. J., 1989, PRL, 62, 376
 Liddle A. R., Wands D., 1991, MNRAS, 253, 637
 Martel H., Wasserman I., 1990, ApJ, 348, 1
 Mathis H., Lemson G., Springel V., et al., 2002, MNRAS, 333, 739
 Mathis H., White S. D. M., 2002, MNRAS, 337, 1193
 McGaugh S. M., Barker M. K., de Blok W. J. G., 2003, ApJ, 584, 566
 Meneghetti M., Bartelmann M., Moscardini L., 2002, preprint, astro-ph/0201501
 Occhionero F., Amendola L., 1994, PRD, 50, 4846
 Occhionero F., Baccigalupi C., Amendola L., Monastra S., 1997, PRD, 56, 7588
 Peacock J. A., 1982, MNRAS, 199, 987
 Peacock J. A., 1999, Cosmological physics, Cambridge University Press
 Peacock J. A., Cole S., Norberg P., et al., 2001, Nature, 410, 169
 Peebles P. J. E., 2001, ApJ, 557, 495
 Peiris H. V., Komatsu E., Verde L., et al., 2003, preprint, astro-ph/0302225
 Percival W. J., Baugh C. M., Bland-Hawthorn J., et al., 2001, MNRAS, 327, 1297
 Perrotta F., Baccigalupi C., Bartelmann M., DeZotti G., Granato G. L., 2002, MNRAS, 329, 445
 Plionis M., Basilakos S., 2002, MNRAS, 330, 399
 Regos E., Geller M. J., 1991, ApJ, 377, 14
 Robinson J., Baker J. E., 2000, MNRAS, 311, 781
 Scoccimarro R., 1998, MNRAS, 299, 1097
 Spergel D. N., Verde L., Peiris H. V., et al., 2003, preprint, astro-ph/0302209
 Springel V., White S. D. M., Tormen G., Kauffmann G., 2001, MNRAS, 328, 726
 Stoehr F., White S. D. M., Tormen G., Springel V., 2002, MNRAS, 335, L84
 Tegmark M., Blanton M. R., Strauss M. A., et al., 2003a, preprint, astro-ph/0310725
 Tegmark M., Strauss M. A., Blanton M. R., et al., 2003b, preprint, astro-ph/0310723
 Tully R. B., Somerville R., Trentham N., Verheijen M. A. W., 2002, ApJ, 569, 573
 van den Bosch F. C., Mo H. J., Yang X., 2003, preprint, astro-ph/0301104
 Verde L., Wang L., Heavens A. F., Kamionkowski M., 2000, MNRAS, 313, 141
 Vikhlinin A., Voevodkin A., Mullis C. R., et al., 2003, ApJ, 590, 15
 Voevodkin A., Vikhlinin A., 2003, preprint, astro-ph/0305549
 Wambsganss J., Bode P., Ostriker J. P., 2003, preprint,

astro-ph/0306088

White S. D. M., 1996, in *Cosmology and Large Scale Structure*, Les Houches Summer School of Theoretical Physics, Session LX, NATO ASI

White S. D. M., Ostriker J. P., 1990, *ApJ*, 349, 22

Will C. M., 2001, *Living Review of Relativity*, 4, 803

This figure "Fig1.gif" is available in "gif" format from:

<http://arxiv.org/ps/astro-ph/0303519v2>

This figure "Fig2.gif" is available in "gif" format from:

<http://arxiv.org/ps/astro-ph/0303519v2>